Enhanced Flexibility of a Bulged DNA Fragment from Fluorescence Anisotropy and Brownian Dynamics

Maddalena Collini,[†] Giuseppe Chirico,[†] Giancarlo Baldini,*[,†] and Marco E. Bianchi[‡]

Dipartimento di Fisica, Istituto Nazionale di Fisica della Materia, Università degli Studi di Milano, via Celoria 16, Milano 20133, Italy, and DIBIT, San Raffaele Scientific Institute, Milano 20132, Italy

Received July 28, 1997; Revised Manuscript Received November 18, 1997

ABSTRACT: A fragment of DNA built from 50 base pairs and two five-adenine unpaired sequences, each inserted in the center of the duplex, has been investigated by measuring the polarization anisotropy decay of intercalated ethidium fluorescence (FPA). When the data from this bulged fragment are compared to those from a straight fully paired duplex or to those from a fragment bent by a five-adenine insertion in one strand, then systematic differences are found in the fluorescence parameters. By employing Brownian dynamics simulations, it is shown that the FPA results from the fragment with the double insertion can be interpreted by assuming a softening of the elastic constant at the bulge. Estimates of the torsion and the bending rigidities at the bulge site are also given.

Introduction

Fluorescence polarization anisotropy (FPA) has proved to be a sensitive technique to investigate the size and the conformation of short DNA fragments labeled with suitable fluorescent probes.[1−3] When short fragments are studied, the most relevant sources of fluorescence depolarization are the rigid body global rotations (spinning and tumbling diffusion) whereas a smaller contribution is given by internal motions dynamics (torsions and bending). In order to better understand the weight of the different contributions, it has been found enlightening to develop proper models of the DNA dynamics to be probed by FPA, since by means of this approach one can extract quantitative information from the experimental data. When regular DNA fragments are considered, suitable and robust analytical theories are available.[4−6] On the other hand, Brownian dynamics (BD) simulations are very useful to analyze FPA data since no accurate analytical model appears to be available for "anomalous" structures. By modeling the DNA as a chain of touching beads, one can show that the FPA correlation function can be successfully predicted from the comparison of simulations and data.

This paper follows the investigation on short DNAs with structural anomalies, which was previously applied[3] to the case of a 50-base pair duplex containing the insertion of an extra five-adenine sequence in one strand and the consequent bending of the structure was established by FPA measurements and BD simulations. Here we apply this analysis to a 50-base pair fragment that contains two sequences of five adenines each inserted in the middle of the duplex and expecting a bulge to occur. While a single insertion has been shown to lead to a stable curvature as the main effect, it is reasonable that the bulge, induced by the double insertion, should enhance the flexibility in the unpaired region.[7] The effect of a 3-base pair bulge on circularization kinetics of small DNA circles has been shown to lead to estimates of the torsional and bending rigidities at the bulge site, which were found to be much lower than those typical of the duplex.[7] The effect of loops and bending on short DNA regions has been examined in recent years with a variety of techniques, such as denaturation kinetics,[8] gel migration,[9] circularization kinetics,[7] fluorescence resonance energy transfer,[10] and fluorescence polarization anisotropy.[3] Bendings and loops are suggested to be correlated to base unpairing and to act by favoring the binding of proteins or the contact between otherwise distant regions of the DNA helix.[11,12]

The aim of the paper is to ascertain whether and to what extent the FPA technique is sensitive to the presence of both dynamic and structural anomalies in short DNA fragments and, by combining the experimental data to BD simulations, to give a quantitative estimate of the induced changes in the DNA elastic properties and the equilibrium structure. The paper first gives a summary of FPA and BD theories. Then, in the Experimental Section, details on the preparation of DNA samples and their sequences are reported. The procedure for FPA measurements and the parameters for BD simulations are shown in the next sections. In the Results and Discussion section, after presentation of the characterization of the two fragments by circular dichroism and UV absorbance melting curves, the FPA data, fitted by a simple mechanical model and by BD simulations, are discussed in detail. The separate contribution of torsional and bending motions to FPA is estimated by means of simulations under different conditions.

Theory

A. Fluorescence Polarization Anisotropy. Fluorescence polarization anisotropy decay of ethidium−DNA complexes has been widely employed in order to gain information on the internal dynamics of nucleic acids.[2,3,13] For this reason, we recall the main concepts of the FPA theory and show here only the most relevant equations. The anisotropy of fluorescence, $r(t)$, can be derived by detecting its time decay at the two standard polarizations (parallel and perpendicular to the vertical polarization of the exciting beam, $I_{\parallel}(t)$ and $I_{\perp}(t)$, respectively). With the exception of very short times when

[†] Università degli Studi di Milano.
[‡] DIBIT.

S0024-9297(97)01136-4 CCC: $15.00
Published on Web 01/17/1998

wobbling may occur (less than 1 ns), the probe can be considered firmly bound to the macromolecule and its binding site geometry well-known. As a consequence, the fluorescence depolarization at different times contains information about the macromolecular motion.

In order to gain quantitative information on the DNA dynamics, one should employ a proper model of the polymer diffusive motions. Some detailed analytical models are available. In this case, a mean cylindrical symmetry for DNA is assumed which is described as a deformable elastic filament[6] with a straight equilibrium structure. A general assumption regarding the uncoupling of intercalating dye wobbling, torsional, and bending motions is made which leads to the expression of the FPA:[6]

$$r(t) = \frac{(I_{||}(t) - I_{\perp}(t))}{(I_{||}(t) + 2I_{\perp}(t))} = r_0 \sum_{n=-2}^{2} I_n(t)C_n(t)F_n(t) \quad (1)$$

This model allows the factorization of the different contributions to the molecular motion: $I_n(t)$ are the internal correlation functions that depend only on the angle between the dye transition dipole and the polymer axis of symmetry (=70.5°) and, since the fluorophore wobbling dynamics spans a range (ps) to which our FPA setup is not sensitive, are essentially time independent. The depolarization due to the fast wobbling is described by a reduced limiting anisotropy factor $r_0 \cong 0.36$. $C_n(t)$ represent the twisting correlation functions, related to torsional motions, whose longest motion is the diffusion spinning around the helix axis: $C_n(t) = \exp[-n^2\langle\Delta\phi_T(t)^2\rangle]$, where $\Delta\phi_T(t)$ is the torsional displacement of the subunits around their z-axes (here identified as the cylinder's long symmetry axis). $F_n(t)$ are the tumbling correlation functions, related to bending motions, whose longest motion is the (doubly degenerate) tumbling motion around an axis perpendicular to the helix axis x: $F_n(t) = \exp[-(6 - n^2)\langle\Delta\phi_B(t)^2\rangle]$, where $\Delta\phi_B(t)$ is the bending angular displacement. Explicit expressions for the correlations functions can be found in ref 2. In the presence of a small free dye contribution, the total anisotropy is given by the intensity-weighted average of the bound and of the free fluorophore.[14] The free dye anisotropy is given by $r_F(t) = r_0 e^{-t/\tau_{rot}}$, where τ_{rot} is taken[15] to be 100 ps and $r_0 = 0.4$.

The FPA data shown in the results section are obtained by detecting the FPA decay in the frequency domain, an alternative method equivalent to the time response.[16,17] It may help, however, to recall some relevant quantities that are directly obtained from the measurements and to show how they compare with eq 1. In the frequency domain, a radio frequency (MHz) modulated beam impinging on a sample forces the fluorescence emission to be modulated at the same frequency, although phase shifted with respect to the excitation and reduced in its relative amplitude (demodulation). Phase shift and demodulation are recorded at each frequency for each polarization direction. It is common to represent the data by collecting the phase shift differences and the demodulation ratios between the two polarizations, namely,

$$\Delta\phi = \phi_{\perp} - \phi_{||} \qquad \Delta M = M_{\perp}/M_{||} \quad (2)$$

these quantities can be related to the Laplace transform of the intensity decays at the two polarization conditions, $L(I_{\perp,||})(\omega)$ in the following way:[15]

$$\mathrm{tg}(\Delta(\omega)) = \frac{\mathrm{Im}(L(I_{\perp})(\omega))\mathrm{Re}(L(I_{||})(\omega)) - \mathrm{Re}(L(I_{\perp})(\omega))\mathrm{Im}(L(I_{||})(\omega))}{\mathrm{Re}(L(I_{\perp})(\omega))\mathrm{Re}(L(I_{||})(\omega)) + \mathrm{Im}(L(I_{\perp})(\omega))\mathrm{Im}(L(I_{||})(\omega))}$$

$$\Delta M(\omega) = \frac{|L(I_{\perp})(\omega)|}{|L(I_{||})(\omega)|} \quad (3)$$

where $\mathrm{Re}(L(I_{\perp,||})(\omega))$ and $\mathrm{Im}(L(I_{\perp,||})(\omega))$ represent the real and the imaginary parts of the Laplace transforms. We recall that $I_{||}(t) = I_{tot}(1 + 2r(t))/3$ and $I_{\perp}(t) = I_{tot}(1 - r(t))/3$. In this way, the fluorescence anisotropy decay in the time domain (eq 1) can be related, through eq 3, to phase differences and demodulation ratios in the frequency domain.[15]

B. Brownian Dynamics. Brownian dynamics simulations have been performed with a FORTRAN program that integrates the Langevin equations for the polymer dynamics with a second-order approximation.[18] The general procedure is based on some basic equations by Ermack and McCammon and Fixman.[19,20] In this paper we adopt the algorithm and the formalism applied by Allison[21] to DNA and further extended by Chirico and Langowski;[22,23] only the essential background is given here.

DNA segments are modeled as a string of touching beads, and the bending and torsional kinematics are described by assigning the positions of the center of each of the M beads and the direction of $M - 1$ reference directions perpendicular to the bonds. The hydrodynamic interactions are described by the the Rotne–Praeger tensor.[24] The coupling of the torsional and bending dynamics is applied as in ref 22. The diffusive molecular properties are introduced in the simulations via the bead's translational diffusion coefficient D_0 and the rotational spinning diffusion coefficient of each bond D_R. The choice of the diffusion coefficient is made by keeping the total volume of the string of beads equal to that of the DNA cylinder. This equivalence has been proposed by Hagerman[25] and gives a satisfying agreement between the tumbling diffusion coefficient of the bead chain and of the corresponding cylinder.[26] As an example, a DNA radius $R = 1.3$ nm would correspond to a string of beads chain with bead's radius $R_{BEADS} = 1.592$ nm. This scaling imposes some coarseness to the model since only DNA lengths proportional to the bead's radius are possible. The spinning diffusion coefficient is more delicate since, instead of the beads, the spinning unit is the bead-to-bead bond. We assume a constraint on the total spinning diffusion of the DNA cylinder. From the torsional Langevin dynamics one would predict a total spinning diffusion for the fragment:

$$D_{spin} = D_R/(M - 1) \quad (4)$$

where D_R is the spinning diffusion coefficient of the single bond. This assumes negligible effect of the bending-torsional coupling on the rigid body spinning dynamics.[22] On the other hand, one knows accurate expressions of D_{spin} such as those given by Garcia de la Torre,[27] where D_{spin} depends on the total DNA length (L) and radius (R):

$$D_{spin} = \frac{K_B T}{[3.841\pi\eta L R^2(1+\delta_{||})]}$$

$$\delta_{||} = (0.677/p) - (0.183/p^2) \quad (5)$$

where $p = L/2R$ is the axial ratio and η is the solution viscosity at temperature T. The D_R value is found by inversion of the equation obtained by comparing the BD (eq 4) and the hydrodynamic (eq 5) values of the spinning coefficient. As an example, for a 50-bp DNA simulated with $M = 5$ beads of $b_0 = 3.184$ nm of diameter and $D_R = 50.15$ MHz, corresponding to the spinning of a rod 0.34 nm high and with a radius of $\cong$0.65 nm.

Harmonic intermolecular potentials take into account the rigidities among the beads through a stretching potential U_s, a bending potential U_b, and a torsional potential U_t. We give for completeness the form of these potentials:

$$U_s = \frac{K_B T}{2\delta^2} \sum_i^{M-1} (b_i - b_0)^2 \tag{6}$$

$$U_b = \frac{K_B T}{2} \sum_{i=1}^{M-2} \frac{1}{\psi_i^2} \beta_i^2 \tag{7}$$

$$U_t = \frac{K_B T}{2} \sum_{i=1}^{M-2} \frac{1}{\xi_i^2} (\alpha_i + \gamma_i)^2 \tag{8}$$

In the formulas, δ is the stretching variance and ψ_i are the bending variances, defined in terms of the polymer local persistence lengths P_i through $\psi_i = (b_0/P_i)^{1/2}$ while the torsional variances, ξ_i, are defined through the local torsional rigidities C_i, $\xi_i = (b_0 K_B T/C_i)^{1/2}$. In this paper, the torsional and bending parameters are position dependent and they are included in the sum over the number of beads in order to make it possible to employ, when needed, different values of and for each bead.

The computation of the FPA correlation function throughout each simulation is accomplished by performing the following average:[3]

$$r_B(j\delta t) = \frac{1}{(N_m - j - 1)} \frac{1}{(M - 1)} \sum_{k=1}^{M-1} \sum_{i=1}^{N_m - j} P_2(\cos(\Phi_{i,j,k})) \tag{9}$$

where P_2 indicates the second Legendre polynomials, N_m is the number of time steps, M is the number of beads, and $\cos(\Phi_{i,j,k}) = \bar{\mu}_k(i + j)\mathrm{d}t)\bar{\mu}_k(i\mathrm{d}t)$ with $\bar{\mu}_k(t)$ indicating the direction of the intercalated ethidium transition dipole at the k-th position.

Experimental Section

A. Materials. DNA oligonucleotides have been synthesized with the phosphotriester method, as previously described,[3,28] and successively purified by gel electrophoresis. The control fragment F0 is obtained by the reaction of seq.0 with seq.0c, yielding a 50-base pair fragment.

seq.0: CCTCGAGAAGCTTCCGGTAGCAGCCCCTTG-
CTAGGACGGATCCCTCGAGG

seq.0c: GGAGCTCTTCGAAGGCCATCGTCGGGGAAC-
GATCCTGCCTAGGGAGCTCC

The bulged fragment F2 is obtained with the same sequence seq.0 synthesized with five extra adenines in the middle (for a total of 55 bases). This sequence seq.5 reacted with a complementary sequence (the same as seq.0c) with the same five extra adenines in its center (seq.5c), as shown below.

seq.5: CCTCGAGAAGCTTCCGGTAG-
CAGCC$\underline{\text{AAAAA}}$CCTTGCTAGGACGGATCCCTCGAGG

seq.5c: GGAGCTCTTCGAAGGCCATC-
GTCGG$\underline{\text{AAAAA}}$GGAACGATCCTGCCTAGGGAGCTCC

We recall that the kinked fragment, which we will refer to as F1 in the results and discussion and previously studied in our laboratory,[3] was obtained by the reaction of seq.5 with seq.0c.

The three different samples have 50 paired bases each; in addition, F1 has a single insertion of five unpaired bases in one strand, while F2 has a double insertion or "bulge" at the center of the double filament. The DNA fragments have been purified by gel electrophoresis for whose detection an aliquot of each preparation was 5′-labeled with [^{32}P]ATP and T4 DNA kinase (Boehringer). Calf thymus DNA from Sigma Chemical Co. has been employed in control measurements when needed. Ethidium bromide (EB) was purchased by Sigma Chemical Co. as a powder and freshly dissolved in the buffer. It was added to DNA samples in the concentration of 1 EB/200 base pairs. Both DNA and EB were dissolved in STE100Mg buffer (10 mM Tris-HCl a pH 7.4, 100 mM NaCl, 5 mM $MgCl_2$, 1 mM EDTA). EB and DNA concentrations were estimated by spectrophotometric measurements in cuvettes of 1-cm optical length and quartz walls. The values of the molar extinction coefficients used were $\epsilon = 6600$ cm^{-1} M^{-1} for DNA at 258 nm and $\epsilon = 5860$ cm^{-1} M^{-1} for EB at 478 nm.

B. Methods. Melting profiles have been acquired with a Lambda 2 (Perkin Elmer) spectrophometer equipped with a thermostated cell holder. The temperature was controlled by a Haake F3 circulating bath and read by a thermocouple in the sample cell. Time-driven scanning of the absorbance was used to check the stabilization of the system at a given temperature; then the spectrum was recorded.

Circular dichroism spectra were recorded with a Jasco J-500A spectropolarimeter directly interfaced to a personal computer. Each acquisition is the average of 40 data points at each wavelength with a spacing of 1 nm.

Fluorescence polarization anisotropy decay measurements have been obtained with a frequency domain K2-ISS (Urbana, IL) fluorometer operated in the range from 1 to 40 MHz. Light excitation was accomplished by the green 514.5-nm output of an argon ion laser (Spectra Physics 2025) employing a power of 500−700 mW. For further details, see ref 15. Digital data acquisition and storage was provided by the ISS-A2D ACD card inserted in a personal computer. For each set of data, 25 logarithmically spaced frequencies are employed in the range 1−40 MHz with a cross-correlation frequency of 80 Hz. A 550-nm long-pass filter was used to cut the scattered light from excitation. The temperature was kept nearly constant by a Haake F3 thermostating bath and directly checked by a thermocouple inserted in the cell compartment which gave the value of $T = 24.5$ °C.

Data are analyzed according to a FORTRAN routine.[3] The number of the fitting parameters is dependent on the fitting model; however, EB lifetimes are always kept at 22.5 ns and at 1.8 ns for the bound and the free species, respectively. Data fitting is accomplished by minimizing the total χ^2, i.e., the sum of the square of the normalized differences between the experimental and computed phase differences and modulation ratios. The trial phase differences and modulation ratios are the Laplace transform of the fluorescence intensities obtained from either an analytical r(t) for the flexible joint model or a simulated $r(t)$ for the BD simulations (see eq 1).[3]

Brownian dynamics simulations have been performed on a HP 9710 Apollo workstation and on Cray C92 (Cineca, Istituto Nazionale di Fisica della Materia) with FORTRAN 77 programs developed in our laboratory.[22,23] BD simulations have been obtained by computing trajectories of 750.000 steps, each time step being of 6.7 ps, for a total of 5000 ns, in order to calculate the fluorescence polarization anisotropy decay correlation function which becomes negligible at times longer than 200 ns. For each simulation, the following values of the parameters have been kept fixed: solution temperature $T =$

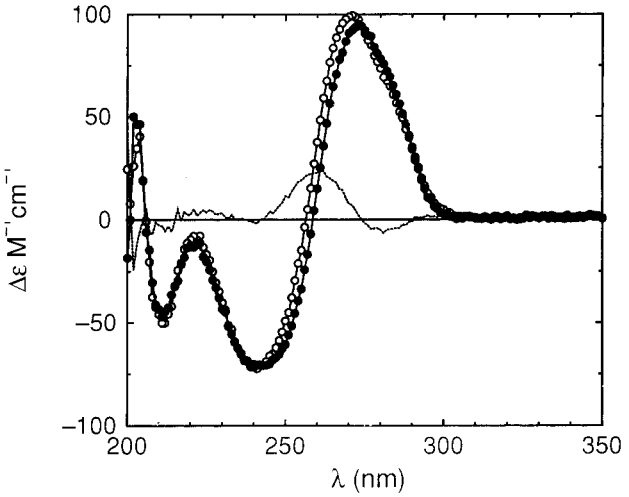

Figure 1. Molar ellipticity of the reference F0 fragment (open circles) and of the double-inserted F2 fragment (filled circles) versus wavelength. The dotted line represents the difference between the two spectra.

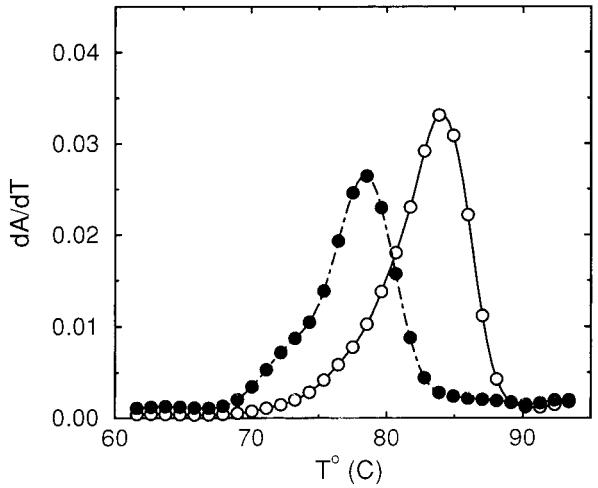

Figure 2. Differential UV absorption at 258 nm versus temperature for the reference F0 (open circles) and the double-inserted F2 fragment (filled circles).

297.15 K, solution viscosity 0.9111 cp, and stretching parameter 0.01, which has been found suitable[22] to keep the DNA contour length constant within ≅2%. The number of monomers units, M, the bead diameter size b_0, and the bond spinning diffusion coefficient are determined for each choice of the DNA length and radius as illustrated in the Results and Discussion section. The value of the torsional rigidity C (appearing in the BD as the parameter) and the value of the persistence length P (defined through the parameter) are assigned to each angle.

Results and Discussion

A. Fragment Characterization. Circular dichroism data of the reference F0 and of the bulged fragment F2 are shown in Figure 1 from 320 to 200 nm. For both samples, a B-structure pattern is apparent though a small shift is found in the positive to negative crossing points of the ellipticity, being at ≈260 nm for F0 and at ≈264 nm for F2. This shift corresponds to a lower ellipticity of the fragment F2 that has five unpaired bases.[29]

A notable difference between the two fragments is found when the thermal stability of the double helix is measured. Under the presence of 5 mM magnesium added to the buffer, both fragments are found to keep their bases paired up to fairly high temperatures ($T >$ 70 °C), with F0 showing a "melting" temperature of 82.7 ± 0.3 °C, while F2 melts at 75.6 ± 0.15 °C, as can be seen in Figure 2. Calf thymus DNA (nearly the same CG content as F0, 64%) in the same buffer melts at 85 ± 0.3 °C. From the values of the enthalpy and entropy changes derived from the melting profile of each fragment, one estimates that the enthalpy difference for the two fragments is $\Delta H_{F0} - \Delta H_{F2} = 11.3 \pm 1$ kcal/mol. Since the disruption of a base pair requires 1.6−1.8 kcal/mol,[29,30] then the lower value of the enthalpy change for F2 is compatible with fewer paired bases, six to seven, when compared to F0. Since F2 has 55 base pairs, while F0 has 50, it is likely that the "bubble" in the middle of the fragment can start nucleation of the denaturation and that probably 2 or 3 base pairs adjacent to the bubble are not paired. In particular when the dependence of the melting temperature on fragment length[31] is being estimated as $1/T_M = a + b/n$, where n is the number of base pairs, the melting temperature difference between a 50- and a 25-base pair duplex, ≈12 °C, is expected to be compared to the observed difference, ≈7 °C. The bulged fragment considered equivalent to two 25-bp independent arms is certainly an oversimplification, but it helps in understanding how a nucleation in the middle can affect the thermal stability of the sample.[10] The linking of the two arms is expected to increase the melting temperature, and this is in agreement with our experimental findings.

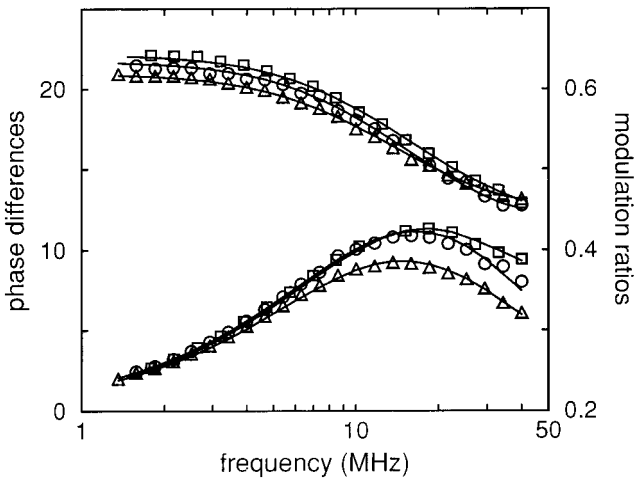

Figure 3. FPA data for the reference F0 (circles), the single-inserted F1 (triangles), and the double-inserted F2 (squares) fragments. Phase differences, lower data, and modulation ratios, upper data, are shown versus the modulation frequency. The continuous lines represent Brownian dynamics simulations fitted to the experimental data, according to the following parameters: for F0, $R = 1.1$ nm, $P = 200$ nm, $C = 2.55 \times 10^{-19}$ erg, $r_0 = 0.367$, and $I_F = 0.02$; for F1, $R = 1.1$ nm, $P = 200$ nm, $C = 2.55 \times 10^{-19}$ erg, $r_0 = 0.33$, $I_F = 0.02$, and bending angle $\theta = 45°$; for F2, $R = 1.1$ nm, $P = 200$ nm, $C = 2.55 \times 10^{-19}$ erg, $P_B = 1000$ nm, $C_B = 0.64 \times 10^{-19}$ erg, $r_0 = 0.37$, and $I_F = 0.017$.

B. Fluorescence Polarization Anisotropy. FPA data in the frequency domain are shown in Figure 3. Both phase difference and demodulation ratios are found to be higher for fragment F2 than for the reference fragment F0. Also shown in the figure for comparison are the FPA data for the single-bulged fragment, labeled F1, previously studied in our laboratory. This fragment, which has the extra five-adenine run on one strand only, was shown[3] to be bent by ≈45°.

The curious feature of the FPA data is that the two modified fragments have opposite trends with respect to the reference. As already recognized for the bent fragment, it will be shown that this behavior is related to both the dynamic and structural features of the samples. In this way, an inspection of the phase and modulation data allows a preliminary qualitative prediction of the dynamical properties of the samples. The continuous lines in Figure 3 represent best fits obtained by BD simulations and will be discussed later.

The analytical fit of the FPA decay by means of the Schurr model (eq 1) gives information on fragment properties such as radius and torsional rigidity constant $\alpha = C/h$ (h is the base pair thickness) and on the intercalated dye features, i.e., the limiting anisotropy r_0 and the free dye fractional intensity I_F.[1,2,13] For the reference fragment F0, a radius $R = 1.08 \pm 0.03$ nm and a torsional constant $\alpha = (7 \pm 1) \times 10^{-12}$ erg result. This kind of analysis had been previously performed also on the kinked fragment F1, when properly taking into account the rigid body spinning and tumbling diffusion coefficients, modified according to the fragment bending. As a result, an estimate of the bending angle, $\theta \approx 45°$, was obtained.[3] The same fitting, applied to the double-bulged fragment F2, yields radius values close (although slightly smaller) to that of the reference and lower values for the torsional constant $\alpha = (6 \pm 1) \times 10^{-12}$ erg . It is therefore likely that a change of the rigid body rotations is not the most relevant feature and that the internal dynamics of the F2 fragment is different from that of the reference fragment. This shows that FPA measurements are sensitive to different types of anomalies in short DNA fragments.

We try in the following to rationalize the possible effect of the "bubble" on the DNA internal dynamics by analyzing the FPA data. This is somehow intriguing since the opposite behavior of the two "anomalous" fragments F1 and F2 could indicate the distinction between a static and a dynamic character of their curvature in solution. Before attempting a description of the data by means of time-consuming and sophisticated Brownian dynamics simulations, one could attempt to analyze the fluorescence anisotropies with a simple and essential model.

C. Flexible Joint Model. We have seen above that a preliminary analysis of the FPA data suggests a perturbation of the internal dynamics of the F2 fragment with respect to F0. Due to the F2 base sequence, one expects a double bulge in the middle of two 25-bp arms, a structure that can be modeled by two cylindrical arms linked by a softer joint. The flexibility of this joint has two components: torsion, which allows one rod to spin around its axis, and bending, which changes the angle between the two rods. In order to give a simple analytical expression of the FPA decay according to this tentative model, it has been assumed that the "rigid" body decay is that corresponding to the equilibrium conformation of the fragment. Permanent bents induce a change mostly in the spinning diffusion coefficient, while dynamic anomalies such as a soft joint are mimicked by damped bending and torsional springs which simply add to the other depolarization contributions. A highly flexible joint should make the coupling of the internal dynamics of the two halves of the DNA fragment very weak: we assume therefore, as a crude approximation, that the internal dynamics of DNA can be described by that of the two separated halves.

In general, the FPA decay can be written as a sum of torsional and bending depolarization factors[6] of the type $C_n(t) = e^{-n^2\langle\Delta\varphi_T(t)^2\rangle}$ and $F_n(t) = e^{-(6-n^2)\langle\Delta\varphi_B(t)^2\rangle}$ (see eq 1), where $\Delta\varphi_T(t)$ and $\Delta\varphi_B(t)$ are the angular displacements experienced by the dye, due to the torsional and bending dynamics of the DNA, respectively. Each of these displacements is composed of a contribution from the internal DNA dynamics,[2,5] from the rigid rod diffusion and, likely, from the flexible joint dynamics:

$$\langle\Delta\phi_T(t)^2\rangle = D_{SPIN}t + \langle\Delta\phi_T^{internal}(t)^2\rangle + \langle\Delta\phi_T^{JOINT}(t)^2\rangle$$
$$\langle\Delta\phi_B(t)^2\rangle = D_{TUMB}t + \langle\Delta\phi_B^{internal}(t)^2\rangle + \langle\Delta\phi_B^{JOINT}(t)^2\rangle \quad (10)$$

All together this leads to polarization losses of the fluorescence light of the type (see eq 1):

$$r(t) = r_0\sum_{n=0}^{2} e^{-n^2D_{SPIN}t}C_{J,n}(t)C_n(t)e^{-(6-n^2)D_{TUMB}t}F_{J,n}(t)F_n(t) \quad (11)$$

where the functions $C_n(t)$ and $F_n(t)$ are the torsional and bending anisotropy contributions, respectively, due to the internal dynamics of each half of the molecule. In particular, $C_{J,n}(t)$ and $F_{J,n}(t)$ are the contributions from the joint,[6] $C_{J,n}(t) = e^{-n^2\langle\Delta\varphi_T(t)^2\rangle}$ and $F_{J,n(t)} = e^{-(6-n^2)\langle\Delta\varphi_B(t)^2\rangle}$. Their mean square displacements can be written as[32]

$$\langle\Delta\varphi_B(t)^2\rangle = 2\sigma_B{}^2(1 - e^{-t\Gamma_B}) \quad (12a)$$

$$\langle\Delta\varphi_T(t)^2\rangle = 2\sigma_T{}^2(1 - e^{-t\Gamma_T}) \quad (12b)$$

where the two relaxation rates Γ_B and Γ_T are closely related to the variance of the angular displacements σ_B and σ_T and to spinning and tumbling diffusion coefficients D^0_{SPIN} and D^0_{TUMB} of the two DNA halves as $\Gamma_T = D^0_{SPIN}/\sigma_T{}^2$ and $\Gamma_B = D^0_{TUMB}/\sigma_B{}^2$.

The parameters affecting the depolarization anisotropy are therefore the DNA torsional constant α, its length and its radius. D_{SPIN} amd D_{TUMB} are the overall spinning and tumbling diffusion coefficients, respectively: they are either computed according to the Garcia de la Torre equations for a rigid rod[27] or used as free parameters of the fit. Two additional parameters are the bending and torsional variances of the angular displacements of the dye due to the motion about the joint.

In fitting the FPA data from the "straight" fragment F0 used as reference, we used eq 11 with no joint, i.e., $C_{J,n}(t) = 1$, $F_{J,n}(t) = 1$, and $(N + 1) = 50$. The FPA data from the F2 and F1 fragments are then fitted by keeping the same radius R, and same torsional constant as found for the straight fragment, but by assuming the presence of a joint and/or by fitting the tumbling and spinning diffusion coefficients. The results are summarized in Table 1.

When the bulged F2 fragment is analyzed, the parameters found for the flexible joint are given by $\sigma_T{}^2 = 0.014$, which corresponds to an equivalent torsional rigidity of $C = h\alpha = h\,(K_BT)/\sigma_T{}^2 \cong 3 \times 10^{-20}$ erg cm, almost 7-fold smaller than the usual one, while the low value for the bending angle variance $\sigma_B{}^2 \approx 10^{-3}$ indicates that with this simple and approximated model no appreciable bending of the joint is apparent. For comparison, a fit of the F1 fragment data yields a

Table 1. Fragment Parameters for FPA Fits by the Flexible Joint Model: DNA Radius *R*, Torsional Elastic Constant α, Spinning D_{SPIN} and Tumbling D_{TUMB} Diffusion Coefficients, Torsional σ_T and Bending σ_B Angular Displacement Variances due to the Flexible Joint, and Reduced χ^2 [a]

fragment	*R* (nm)	α × 10^{12} (erg)	D_{SPIN} (MHz)	D_{TUMB} (MHz)	σ_T^2	σ_B^2	χ^2
F0 (straight)	1.1	7.8	17.2	1.35			2.8
F2 (bulged)	1.1*	7.8*	17.2	1.35	0.023	$<10^{-3}$	3.2
F1 (bent)	1.1*	7.8*	11.8	1.61			1.6

[a] The asterisks indicate the parameters that have been kept fixed during the fitting procedure.

substantially lower value of the spinning diffusion coefficient and a larger one of the tumbling coefficient. These values are compatible with a fragment bending angle of ≅45° as previously found. When, instead, the radius is a fitting parameter, values larger than that of F0 are found ($R = 1.27$ nm), again indicating a greater encumbrance of F1 due to its curved structure (data not shown). The excellent fits of FPA data obtained with the joint model are almost coincident with those of the Brownian dynamics shown in Figure 3.

D. Brownian Dynamics Simulation. The treatment given in the previous paragraph, by means of the simple joint model, suggests the presence of a torsional-bending joint possibly coupled to a permanent bend. The effect of such a structural and dynamic anomaly on the FPA decay can be predicted in some detail by BD simulations, which also takes into account the internal motions. However, qualitative information can be obtained from known studies of the hydrodynamics of bent or broken rods, according to rigid body treatments of either the average or the instantaneous molecular configurations.[33] Two different rotational diffusion times are identified: one related to the rotation of the whole molecular structure and the other to the rotation of the smallest rigid segment of the macromolecule. A comparison to BD simulations shows that the FPA decay is not a single exponential, and furthermore, it is affected by both the rigid body rotation and the flexibility of the bending joints. In order to account properly for the torsional-bending joint and the rigid body rotation, BD simulations have been used to reproduce the FPA decay of the fragments under investigation, as previously done with the bent one. In this case, the bent equilibrium structure of the fragment was obtained by means of an additional "kink" potential, and good agreement was found between data and simulations.[3] A DNA fragment is modeled as a chain of *M* touching beads whose diameter is equal to the bond length, b_0. The number of Euler angles to be specified is $(M - 2)$, and for each angle, different values of the bending and of the torsional parameters can be separately assigned. In the case of the reference duplex, F0, the values of the rigidities are the same all over the chain (uniform chain). The bulged duplex F2, instead, can be simulated by employing values of the bending and torsional rigidities of the central bond lower than those of the whole chain.

In Figure 4, FPA simulated data for "bulged" chains are shown together with the FPA of a uniform one (continuous lines). The dotted lines show the results for a chain that has been modified by a 4-fold weaker torsional rigidity of the center of the chain, whereas the dashed lines refer to a chain modified by a 4-fold weaker bending flexibility. It is rewarding that the trend of the simulated data agrees well with the behavior of the experimental FPA: both phase and modulation values are higher for the simulated bulged chains than those for the reference uniform chain. Moreover, one notices

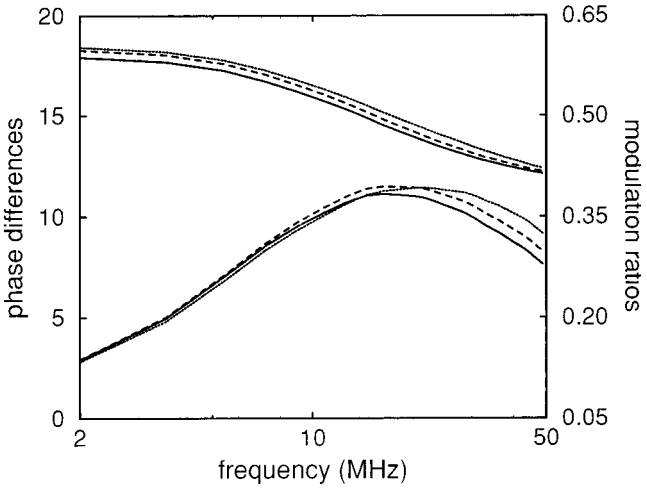

Figure 4. FPA data from BD simulations versus the modulation frequency. Phase differences are shown in the lower part of the figure while modulation ratios are shown in the upper part. The simulations were obtained according to the following parameters: the continuous lines represent the uniform chain with $P = 200$ nm $C = 2.55 \times 10^{-19}$ erg, $M = 5$, and $b_0 = 3.184$ nm. The dotted lines represent a chain with a torsional joint with the same parameters as those of the uniform one and $C_B = C/4$; the dashed lines represent a chain with a bending joint with the same parameters as those of the uniform one and $P_B = P/4$.

that the effect of a purely torsional joint is also that of shifting the maximum in phase differences values to higher modulation frequencies when compared to the uniform chain curve. By computing the spinning and tumbling diffusion coefficients for several configurations that have been sampled at random from the above BD simulations, it appears that a purely torsional joint does not appreciably modify the rigid body rotations of the duplex, while a flexible bending joint has considerable effect. In this case, in fact, spinning is slower and tumbling is faster than in the reference "straight" fragment. This effect, however, is much less pronounced than in the case of the kinked F1 duplex, where, for instance, the spinning diffusion coefficient was found substantially (40%) lower than that of F0.[3] The similarity of the FPA data of the F2 fragment and the flexible joint BD simulations suggests a relevant local perturbation of the DNA internal dynamics.

For this reason, it is interesting to analyze separately the effect of a torsional and bending joint on either the torsional or the bending internal dynamics. If a fluorescent probe were intercalated with its dipole parallel to the helix axis, then the dipole trigonometric orientation factors would cancel the twisting correlation functions and, consequently, the detection of spinning and torsion. Only bending and tumbling would depolarize the emission in this case. By simulating FPA decay correlation function with such a probe, ($\epsilon = 0°$), one could predict the contribution of the bending motions alone to FPA, as shown in Figure 5A. FPA simulations

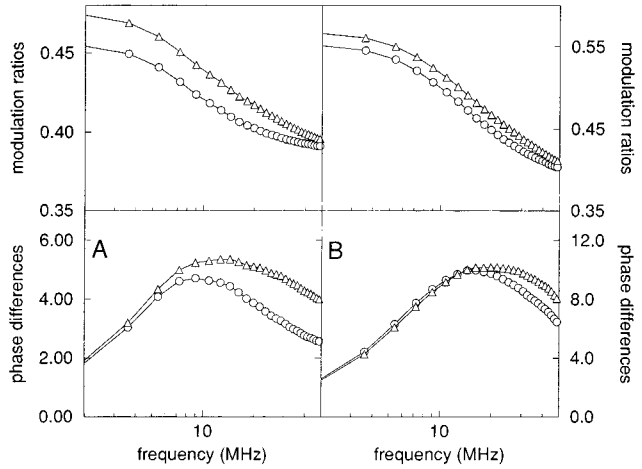

Figure 5. Effect of a torsional and bending joint on the simulated FPA. The uniform chain (circles) is simulated with $M = 5$, $b_0 = 3.184$ nm, $P = 200$ nm, and $C = 2.55 \times 10^{-19}$ erg. The bulged chain is simulated with the parameters of the uniform chain and $C_B = C/4$ and $P_B = P/4$ (triangles). Phase differences data are shown in the lower part of the figure, while modulation ratios are shown in the upper part versus the modulation frequency: (A) Effect on the bending dynamics. The two data sets are obtained by setting the transition dipole angle of the fluorescent probe parallel to the helix axis, $\epsilon = 0$. (B) Effect on the torsional dynamics. The two data sets are obtained by freezing the bending motions as explained in the text.

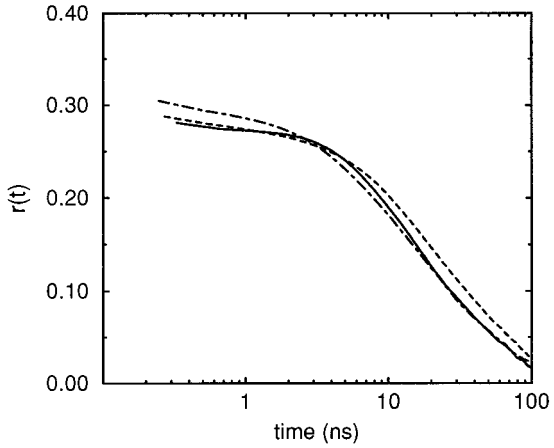

Figure 6. Bound and free EB contribution to fluorescence anisotropy decay $r(t)$ versus time. The three curves represent the Brownian dynamics fits to frequency domain FPA data as discussed in Figure 3: continuous line, F0; dashed line, F1; dot−dashed line, F2.

for a uniform and for a bulged chain, where torsional and bending rigidities are reduced 4-fold at the bulge site, are shown in the figure. The trend is again similar to that found for the experimental data, though enhanced, suggesting a substantial role played by the bending modes in the bulged chain.

In order to follow only the torsional dynamics of the fragments, we performed BD simulations for the uniform and the bulged chain with frozen bending motions. In this case in fact, the bending motions appear in the FPA expression (eq 1) at all the values of ϵ. The corresponding FPA simulated curves in the frequency domain are shown in Figure 5B. Here again it is found that the trend in the simulated chains agrees with the experimental data. The minor differences between the two sets of simulated points show that the effect of the bulge is somewhat smaller on the torsional dynamics than on the bending dynamics. However, it is apparent from Figure 5 that both internal motions give a significant contribution to FPA.

In order to analyze the experimental FPA data more quantitatively, some parameters employed for simulating the uniform chain F0 have been kept fixed. Throughout this work we have chosen to keep the persistence length at the value of $P = 200$ nm since this value is generally taken to be the most likely,[34] and moreover, the studied duplexes are short enough not to be influenced by its exact value ($L/P < 0.1$). On the contrary, since the torsional rigidity is usually a parameter that is determined from FPA data fitting, in the simulations we have chosen to employ three different values, corresponding to $C = 1.7 \times 10^{-19}$, $C = 2.55 \times 10^{-19}$, and $C = 3.4 \times 10^{-19}$ erg cm. We recall that the torsional rigidity constant C is related to the torsional elastic constant per base pair (the quantity directly determined by an analytical fit) by $C = h$, where h is the rise per base pair along the helix axis. The employed values are $\alpha = 5 \times 10^{-12}$, 7.5×10^{-12}, and 10×10^{-12} erg. A least-squares fitting was then run on FPA data with the simulated FPA correlation functions: the adjustable parameters, the limiting dye anisotropy and the free dye fractional contribution, are enclosed in the time FPA decay before operating its Fourier transform. Phase differences and demodulation ratios are then computed to compare them to the experimental data.

In order to ascertain which value of the spinning radius R better describes the experimental data, in addition to the commonly reported BD value $R = 1.3$ nm, corresponding to $b_0 = 3.184$ nm (i.e., 9.4 base pairs), we employed also $R = 1.1$ nm corresponding to $b_0 = 2.694$ nm and $R = 1.0$ nm corresponding to $b_0 = 2.450$ nm. The number of beads units employed for the different bead size values was $M = 5$, 6, and 7, respectively. The best χ^2 values for fragment F0 are obtained with a DNA radius of 1.1 nm and uniform rigidity constant values in the range $1.7 \times 10^{-19} \leq C \leq 2.55 \times 10^{-19}$ erg cm corresponding to torsional constants $5 \times 10^{-12} \leq \alpha \leq 7.5 \times 10^{-12}$ erg. The r_0 values fall between 0.360 and 0.375 while I_F ranges between 0.01 and 0.02.

For each uniform chain simulation, we have tried a range of likely bulge site rigidities, P_B and C_B, at the central chain angle in order to represent the bulged fragment F2. The values that result in good χ^2 values are those obeying the relations $P_B < P$, $C_B < C$, and $P_B C_B \approx PC/10$, where the values for P and C are those found for the reference fragment F0. The continuous lines in Figure 3 represent best fits obtained with the BD simulation superimposed to the experimental FPA data. For sake of comparison to the time domain results, we also reported in Figure 6 the fluorescence anisotropy decays $r(t)$ corresponding to the fitting modulations and phase shifts shown in Figure 3.

Since in the bead model adopted for the simulation requirements the bulge size comes out larger than the expected size (8−9.4 bp out of 47 bp instead of 5 bp out of 50 bp), then the bulge site rigidities values should be rescaled by the ratio between the simulated and the actual bulge sizes. We can estimate the scaling factor by considering that two DNA stretches comprising N and M bases should give similar depolarization when the mean square angular displacements per base pairs are in the relation $N\langle\vartheta_N^2\rangle = M\langle\vartheta_M^2\rangle$. Since the elastic constants (α or P) are inversely proportional to the mean

square angular displacements, one can therefore estimate a scaling factor approximately given by the ratio of base pairs in the two DNA stretches. Our estimate of the bulge torsional and bending rigidities are therefore to be scaled by the factor $\cong 9/5 \cong 1.7$, yielding $P_B C_B \approx PC/(10 \times 1.7^2) \cong PC/30$.

From the above simulations, one finds how a run of unpaired bases modifies the dynamics of a DNA fragment. This appears to be in agreement with experiments of circularization made on small circular DNA, less than 200 base pairs, with or without bubbles which clearly revealed enhanced flexibility, of both torsional and bending character.[7] It has been also shown that while a stable bending in the helix axis could produce a large electrophoretic retardation (this is the case for F1 fragment), a bulged duplex may present a small electrophoretic anomaly,[7] probably due to the larger flexibility at the bulge that allows some rearrangement of the helix structure when passing through the gel matrix. The above discussion suggests that FPA, when coupled with BD simulations, can be successfully employed to describe unusual DNA structures and, in conclusion, the following points can be summarized:

1. The presence of unpaired regions in short fragments can be revealed by lower temperature melting curves probably due to enhanced nucleation.

2. By simply inspecting the trend of phase and modulation versus frequency, FPA data allow one to distinguish the dynamic behavior of short DNA fragments without resorting to complex models.

3. A semiquantitative prediction of the lower rigidity at the bulge site can be obtained by employing a simple mechanical model of a flexible joint.

4. With Brownian dynamics simulations, it is also possible to separate the effects of the bulge on the torsional and on the bending dynamics. In particular, the bending motion has been shown to remarkably affect the dynamics in short fragments also.

5. The comparison between the single- and the double-inserted fragments reveals that the two "anomalies" give different conformations: a permanent bend is created by the single insertion ("static curvature") while a flexible joint is made by the double insertion ("dynamic curvature").

Acknowledgment. This work has been partially supported by Consiglio Nazionale delle Ricerche (C.N.R.) and by Istituto Nazionale di Fisica della Materia (INFM) with a grant on the Cray C92 of CINECA (Bologna, Italy). We thank Elvira Meroni for her help during measurements.

References and Notes

(1) Fujimoto, B. S.; Miller, J. M.; Ribeiro N. S.; Schurr, J. M. *Proc. SPIE-Int. Soc. Opt. Eng.* **1992**, *1922*, 360 (*Laser Study of Macroscopic Biosystems*).
(2) Nuutero, S.; Fujimoto, B. S.; Flynn, P. F.; Reid, B. R.; Ribeiro N. S.; Schurr, J. M. *Biopolymers* **1994**, *34*, 463.
(3) Collini, M.; Chirico, G.; Baldini, G.; Bianchi, M. E. *Biopolymers* **1995**, *36*, 211.
(4) Barkley, M. D.; Zimm, B. H. *J. Chem. Phys.* **1979**, *70*, 2991.
(5) Allison, A.; Schurr, J. M. *Chem. Phys.* **1979**, *41*, 35.
(6) Schurr, J. M. *Chem. Phys.* **1984**, *84*, 71.
(7) Kahn, J. D.; Yun, E.; Crothers, D. M. *Nature* **1994**, *368*, 163.
(8) Crothers, D. M.; Spatz, H. C. *Biopolymers* **1971**, *10*, 1949.
(9) Battacharyya, A.; Lilley, D. M. *Nucleic Acid Res.* **1989**, *17*, 6821.
(10) Lilley, D. M.; Clegg, R. M. *Quat. Rev. Biophys.* **1993**, *26*, 131.
(11) Harrington, R. E. *Mol. Microbiol.* **1992**, *6*, 2549.
(12) Rippe, K.; von Hippel, P.; Langowski, J. *Trends Biochem. Sci.* **1995**, *20*, 500.
(13) Wu, P.; Fujimoto, B. S.; Schurr, J. M. *Biopolymers* **1987**, *26*, 1463.
(14) Lakowicz, J. R. *Principles of Fluorescence Spectroscopy*; Plenum Press: New York, 1983.
(15) Collini, M.; Chirico, G.; Baldini, G. *Biopolymers* **1992**, *32*, 1447.
(16) Weber, G. *J. Chem. Phys.* **1977**, *66*, 4081.
(17) Lakowicz, J. R.; Maliwal, B. P. *Biophys. Chem.* **1985**, *21*, 61.
(18) Iniesta, A.; Garcia de la Torre, J. *J. Chem. Phys.* **1990**, *92*, 2015.
(19) Ermak, D. L.; McCammon, J. A. *J. Chem. Phys.* **1978**, *69*, 1352.
(20) Fixman, M. *J. Chem. Phys.* **1978**, *69*, 1527.
(21) Allison, S. A. *Macromoleculas* **1986**, *19*, 118.
(22) Chirico, G.; Langowski, J. *Biopolymers* **1994**, *34*, 415.
(23) Chirico, G. *Biopolymers* **1996**, *38*, 201.
(24) Rotne, J.; Praeger, S. *J. Chem. Phys.* **1969**, *50*, 4831.
(25) Hagerman, P. J.; Zimm, B. H. *Biopolymers* **1981**, *20*, 1481.
(26) Collini, M.; Chirico, G.; Baldini, G. *J. Chem. Phys.* **1996**, *104*, 6058.
(27) Garcia De La Torre, J.; Bloomfield, V. A. *Q. Rev. Biophys.* **1981**, 81.
(28) Bianchi, M. E. *EMBO J.* **1988**, *7*, 843.
(29) Marky, L. A.; Kallenbach, N. R.; McDonough, K. A.; Seeman, N. C.; Breslauer, K. J. *Biopolymers* **1987**, *26*, 1621.
(30) Marky, L. A.; Breslauer, K. J. *Biopolymers* **1987**, *26*, 1601.
(31) Cantor, C. R.; Schimmel, P. R. *Biophysical Chemistry*; W. H. Freeman and Co.: San Francisco, 1980.
(32) Doi, M.; Edwards, S. F. *The theory of polymer dynamics*; Clarendon Press: Oxford, U.K., 1986.
(33) Garcia De La Torre, J. *Eur. Biophys. J.* **1994**, *23*, 307 and references therein.
(34) Song, L.; Schurr, J. M. *Biopolymers* **1990**, *30*, 229.

MA971136T